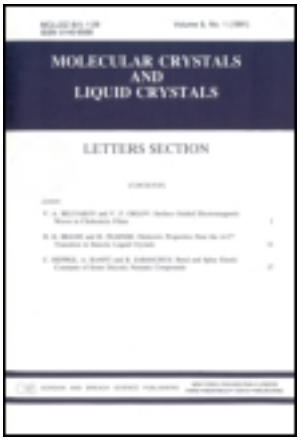

Molecular Crystals and Liquid Crystals
Publication details, including instructions for authors and subscription information:
http://www.tandfonline.com/loi/gmcl20

Theoretical Basis of Novel Liquid Crystal Displays Using Electric Birefringence Effect

Masahiro Kosuge [a c], Shohei Naemura [b] & Kaoru Fujimura [a]

[a] Department of Mechanical and Aerospace Engineering, Graduate School of Engineering, Tottori University, 4-101, Koyama-Minami, Tottori, 680-8552, Japan

[b] Tottori University Electronic Display Research Center, Faculty of Engineering, Tottori University, 4-101, Koyama-Minami, Tottori, 680-8552, Japan

[c] Japan Display West Inc., 1-3-11 Fukashi, Matsumoto, Nagano, 390-0815, Japan

Published online: 16 Dec 2013.

To cite this article: Masahiro Kosuge, Shohei Naemura & Kaoru Fujimura (2013) Theoretical Basis of Novel Liquid Crystal Displays Using Electric Birefringence Effect, Molecular Crystals and Liquid Crystals, 583:1, 85-103, DOI: 10.1080/15421406.2013.844292

To link to this article: http://dx.doi.org/10.1080/15421406.2013.844292

Mol. Cryst. Liq. Cryst., Vol. 583: pp. 85–103, 2013

ISSN: 1542-1406 print/1563-5287 online
DOI: 10.1080/15421406.2013.844292

Taylor & Francis
Taylor & Francis Group

Theoretical Basis of Novel Liquid Crystal Displays Using Electric Birefringence Effect

MASAHIRO KOSUGE,[1,3,*] SHOHEI NAEMURA,[2] AND KAORU FUJIMURA[1]

[1]Department of Mechanical and Aerospace Engineering, Graduate School of Engineering, Tottori University, 4-101, Koyama-Minami, Tottori 680-8552, Japan
[2]Tottori University Electronic Display Research Center, Faculty of Engineering, Tottori University, 4-101, Koyama-Minami, Tottori 680-8552, Japan
[3]Japan Display West Inc., 1-3-11 Fukashi, Matsumoto, Nagano 390-0815, Japan

Electric birefringence of nematic liquid crystals in the isotropic phase and the wall effects were analyzed upon a basis of the Landau-de Gennes theory. Obtained phase diagrams explain the electro-optic characteristics of novel liquid crystal displays using electric birefringence very well and the analytical results of wall effects provide qualitative explanation of the effects of substrate surface treatment on the operation voltage. The present analysis is expected to be useful to improve the display performance and optimize the display panel design.

Keywords Electric birefringence; Landau-de Gennes theory; liquid crystal display; phase transition; wall effects

1. Introduction

In response to the strong demand for fast switching liquid crystal displays (LCDs), several proposals of electro-optic mode have been made for nematic LCDs to actualize sub-millisecond response times. A familiar example is to use polymer stabilized blue phases [1], which has also been extended to a vertical field switching mode for uses in color sequential projection displays [2]. Other ideas, for instance, are to use the flexoelectric effect of short pitch cholesteric LCs [3]. Both standing [4] and lying [5] helix configurations are reported and polymer stabilization technologies have also been adapted to these two modes [6,7]. In contrast to those display modes using a deformation of the director field under an applied electric field, a novel concept was also presented to apply an electric-field-induced order-disorder transition to LCDs. Recently, by using the electric birefringence effect associated with this transition, two kinds of basic LC cell structure were reported to exhibit sub-millisecond or even faster responses [8,9]. One is the basic LC cell for uses typically in projection displays, which has the vertical aligned (VA) LCD like structure with electrodes on both substrates. The other basic LC cell has the in-plane-switching LCD like structure

*Address correspondence to Mr. Masahiro Kosuge, Japan Display West Inc., 1-3-11 Fukashi, Matsumoto, Nagano 390-0815, Japan. Tel.: +81-263-87-2038; Fax: +81-263-87-2059. E-mail: masahiro.kosuge.hu@j-display.com

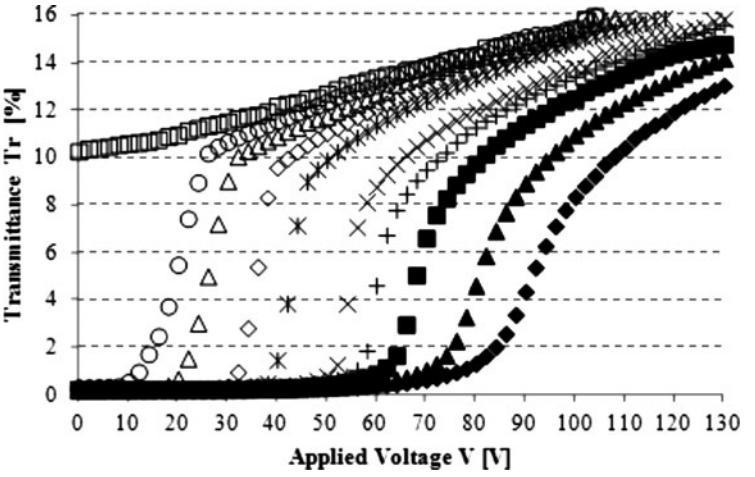

Figure 1. Applied voltage V dependence of the light transmittance of a 3μm-gap homeotropic cell in a wide temperature range ($T = T_{NI}$-0.3(□), ±0(○), +0.1(△), +0.3(◇), +0.5(*), +0.8(×), +1.1(+), +1.4(■), +2.0(▲), +2.5(♦)[°C]).

with both electrodes on one substrate, which can also be used for direct-view LCDs. In both cases, the LC material used has a positive dielectric anisotropy and the feature is that it is operated at temperatures where the zero-field bulk state is in isotropic liquid phase.

This paper will describe the theoretical basis of these novel LCDs using the electric-birefringence effect of nematic LCs in the isotropic phase and present results of numerical calculations of static characteristics. In the first part, the Landau model of nematic(N)-isotropic(I) phase transition will be used to proceed numerical simulation of the electro-optic characteristics of the LC cell. Next, the Landau phenomenological theory will also be applied to the interfacial region of the LC cell to investigate the observed effects of the substrate surface treatments. In the final part, some concluding remarks will be presented.

2. Phenomenological Theory of Basic Electro-Optic Effect

The electric birefringence (Kerr effect) under a DC (low frequency) field was first studied experimentally by Nicastro and Keyes [10] for dielectrically positive nematics, and the critical point was numerically analyzed by Hornreich [11]. The experimental confirmation of the existence of the critical point and its quantitative examination on a basis of Landau theory was also made by Lelidis and Durand [12]. On the other hand, Nicastro and Keyes [10] observed electric-field-induced critical phenomena of dielectrically negative nematics by using a sandwich microcell with two stripes of metal electrode. For such a system composed of anisotropic molecules prefer to line up transverse to an applied field, the existence of a critical field above which the phase transition is second order was found theoretically by Fan and Stephen [13]. Prior to these studies, as far as the electric birefringence is concerned, the first study was made theoretically by Hanus [14] for the optical Kerr effect on the system composed of anisotropic molecules, which prefer parallel orientation to the acting electric field.

Figure 1 shows the measured applied-voltage (V) dependence of optical transmittance (Tr) with the temperature (T) as a parameter by using a VA-LCD like structured cell

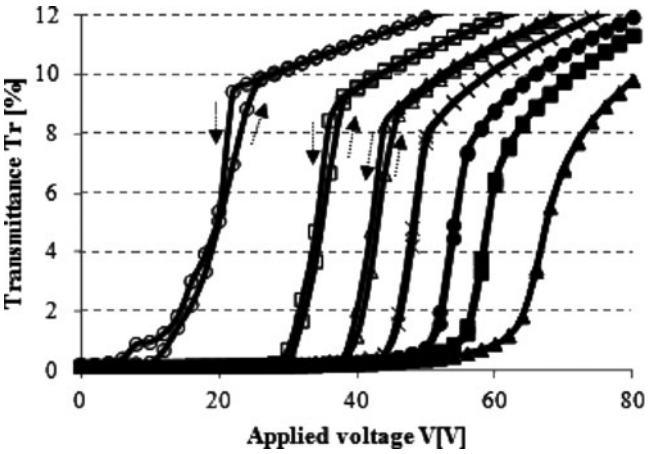

Figure 2. Applied voltage V dependence of the light transmittance of a 3μm-gap homeotropic cell measured in a cycle of increasing and decreasing voltage. ($T = T_{NI} \pm 0$(○), $+0.2$(□), $+0.4$(△), $+0.6$(×), $+\ 0.8$(●), $+1.0$(■), $+1.2$(▲) [°C]). An estimated critical point locates around($T_c = T_{NI} + 0.6\,[^\circ C]$, $E_c = 48[V/3.0\mu m]$).

containing a dielectrically positive LC material, 5CB(4'-*n*-pentyl-4-cyanobiphenyl) [8]. The optical transmittance was measured under crossed polarizers with an incident light angle of 45° from the cell surface normal. Measurements were performed in a range of the reduced temperature $T - T_{NI}$ between -0.3 and $+ 3.0$[°C], where T_{NI} is the zero-field N-I transition temperature (35.3[°C] for 5CB). As a homeotropic surface treatment is applied to the substrate surface, the director is uniformly aligned perpendicular to the substrate surface at a temperature below T_{NI} resulting in around 10% transmittance due to the angle of 45° between the director and the optical path. When a finite amplitude of voltage is applied, a small increase in the transmittance is obtained due to the change of molecular orientational order S under electric field E. On the other hand, when the temperature is above T_{NI} and the LC material is in the I phase ($S = 0$), the transmittance is practically 0% without voltage application because of the optical isotropy of the LC material. As the applied voltage is increased, the optical transmittance gradually increases and makes a big jump at some threshold amplitude V_{th}, which depends on the temperature. This optical transmittance obtained by a voltage application is reasonably understood as a result of an electric birefringence corresponding to the electric field induced orientational order ($S > 0$). The weakly ordered state induced by a voltage below $V_{th}(T)$ can be identified as a para-nematic (pN) phase. From Fig. 1, it is anticipated that a critical point, which is theoretically predicted as mentioned above, locates around $\sim 40 < V <\sim 60$[V] and $\sim 0.5 < T - T_{NI} <\sim 0.8$[°C]. In order to clarify the location of the critical point, where the first order pN-N transition vanishes and the pN phase changes continuously into the N phase, the voltage dependence of the optical transmittance was measured in a cycle of increasing and decreasing voltage. As shown in Fig. 2, a hysteresis is observed in the V-Tr plane in a lower temperature range and vanishes in a higher temperature range. This hysteresis is considered to be caused by the existence of metastable ordered states, which are a metastable pN phase on a voltage-increasing path and a metastable N phase on a voltage-decreasing path. This is also correlated to the fact that the phase transition is of the first order. Thus, from the continuous curve for $T = T_{NI} \pm 0.6$ (×) in Fig. 2, the critical point is estimated to locate around

the point $(T_c, E_c) = (T_{NI} + 0.6\,[^\circ C]\,, 48[V/3.0\mu m]) = \left(35.9\,[^\circ C]\,, 1.6 \times 10^7\,[V/m]\right)$ exhibiting about 5% transmittance which is half of the transmittance for $T = T_{NI}$ -0.3(◊) and $V = 0$ in Fig. 1.

According to the Landau de Gennes theory [15], the free energy density of a nematic system in the presence of a stabilizing electric field E parallel to the uniformly aligned director ***n*** may be written in the I phase as:

$$F = F_0 + \frac{3}{4}a\left(T - T^*(0)\right)S^2 - \frac{1}{4}BS^3 + \frac{9}{16}CS^4 - \frac{1}{3}DSE^2, \tag{1}$$

where F_0 is the free energy density of the electric-field-free I phase. Here, the nematic order S is assumed to be positively uniaxial, $0 \leqq S \leqq 1$, and depends on temperature T and the electric-field strength E. The coefficients a, B, C are supposed constant and positive and $T^*(0)$ represents the zero-field super-cooling limit temperature of the I phase. The coefficient D is assumed to be temperature independent and to be related to the dielectric anisotropy $\varepsilon\varepsilon(\Delta\varepsilon)_0$ of the N phase. Here, $\varepsilon\varepsilon_0$ is the permittivity of a vacuum with the numerical value in rationalized m.k.s. units of 8.854×10^{-12} and $(\Delta\varepsilon)_0$ the relative dielectric anisotropy of a perfectly ordered state ($S = 1$) of the material. That is, the relative dielectric anisotropy of the LC material in the N phase is assumed to be given by $\Delta\varepsilon\,(T) = (\Delta\varepsilon)_0\,S\,(T)$and $D = \varepsilon\varepsilon_0(\Delta\varepsilon)_0$. The zero-field phase transition temperature T_{NI} and the degree of order at this temperature $S_{NI} = S(T = T_{NI})$ are obtained from the stationary condition, $\partial F/\partial S = 0$ and $\partial^2 F/\partial S^2 > 0$, and $F_{S=0} = F_{S=S_{NI}}$ as

$$S_{NI} = \frac{2B}{9C}, \tag{2}$$

$$T_{NI} - T^*\,(0) = \frac{B^2}{27aC}. \tag{3}$$

The degree of order S(T) under a fixed electric field E can be obtained as a root of $\partial F/\partial S = 0$, which gives the global minimum of F, that provides S(T) curves with E as a parameter in the T-S plane. Setting the three real roots of the equation $\partial F/\partial S = 0$ as $S_1 \leqq S_2 \leqq S_3$, the phase transition temperature $T_{N\text{-}pN}(E)$ under an applied electric field E, which corresponds to T_{NI} when $E = 0$, is given by the solution of$(\partial F/\partial S)_{S=S_1} = (\partial F/\partial S)_{S=S_3} = 0$ and $F_{S=S_1} = F_{S=S_3}$, satisfying the equation:

$$S_{3,1} = S_c \pm \sqrt{3S_c^2 - \frac{2a}{3C}(T_{N-pN}\,(E) - T^*(0))}, \tag{4}$$

where + and − corresponds to S_3 and S_1, respectively. Equation (4) provides a coexistence line for both N and pN phases reflecting the first order phase transition in the T-S plane. Here, $S = S_c$ is the degree of order at a critical point, which appears in the phase diagram for $\partial F/\partial S = \partial^2 F/\partial S^2 = \partial^3 F/\partial S^3 = 0$ yielding the following equations:

$$\frac{\partial F}{\partial S}|_{S=S_c} = -\frac{1}{3}DE_c^2 + \frac{3}{2}a\left(T_c - T^*(0)\right)S_c - \frac{3}{4}BS_c^2 + \frac{9}{4}CS_c^3 = 0, \tag{5a}$$

$$\frac{\partial^2 F}{\partial S^2}|_{S=S_c} = \frac{3}{2}a\left(T_c - T^*(0)\right) - \frac{3}{2}BS_c + \frac{27}{4}CS_c^2 = 0, \tag{5b}$$

$$\frac{\partial^3 F}{\partial S^3}|_{S=S_c} = -\frac{3}{2}B + \frac{27}{2}CS_c = 0. \tag{5c}$$

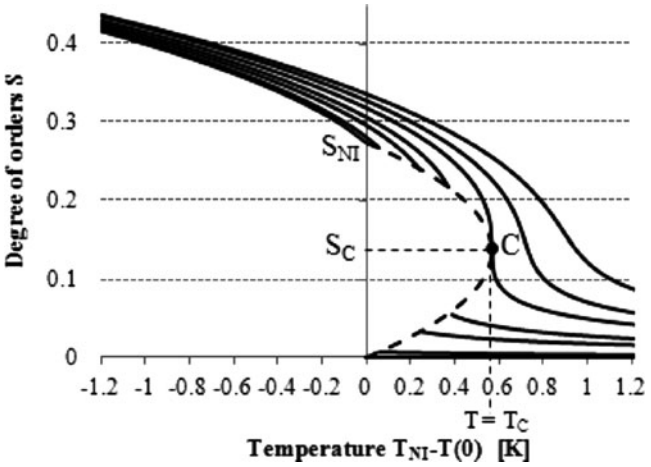

Figure 3. S(T, E) curves with E as a parameter. Full lines correspond to different electric fields E below and above the critical field Ec. C is the critical point (Tc, Sc),which locates on the solid line for E = Ec. The dashed line is the coexistence line of pN (or I for zero-field case) and N phases.

From Eqs. (5a)−(5c), the critical values are analyzed as

$$S_c = \frac{B}{9C} = \frac{1}{2}S_{NI}, \tag{6}$$

$$E_c^2 = \frac{3B}{4D}S_c^2 = \frac{B^3}{108C^2D}, \tag{7}$$

$$T_c - T^*(0) = \frac{B^2}{18aC}. \tag{8}$$

By inserting Eq. (6) into Eq. (4), the equation of the coexisting line can be rewritten as

$$\left(S_{N-pN} - \frac{B}{9C}\right)^2 = \frac{1}{27C^2}[B^2 - 18aC(T_{N-pN}(E) - T^*(0))]. \tag{9}$$

Here, S_{N-pN} corresponds to the two real roots S_3 and S_1 given by Eq. (4). That is, S_{N-pN} is the degree of order S(T, E) specified at the first-order phase transition point with $T = T_{N-pN}$ and $E = E_{N-pN}$ and takes the two values corresponding to bistable pN and N phases.

When a set of experimentally obtained values [16] of the coefficients for 5CB:

$$a = 0.087 \times 10^6\,[J/Km^3],\ B = 2.13 \times 10^6\,[J/m^3],\ C = 1.73 \times 10^6\,[J/m^3] \tag{10}$$

are used, the characteristic temperature T*(0) is calculated to be $T_{NI} - 1.12\,[K] = 34.3[^\circ C]$ and the critical temperature $T_c = T_{NI} + B^2/(54aC) = 35.9[^\circ C]$, as well. Furthermore, by estimating [16] $(\Delta\varepsilon)_0 = 10$, which corresponds to $D = 8.8_5 \times 10^{-11}[F/m]$, the critical electric field E_c is calculated to be $1.8_3 \times 10^7$ [V/m]. The calculated critical point $(T_c, E_c) = (35.9[^\circ C],\ 1.8 \times 10^7[V/m])$ agrees well to the above observation results. The degree of order S is also calculated as $S_{NI} = 0.27_4$ at $T = T_{NI}$ without voltage application and at the critical point as $S_c = 0.14$.

The S(T) curves with E as a parameter are obtained as shown by the full lines in Fig. 3, and the dashed line in Fig. 3 represents the coexistence line of pN phase (I phase in case of

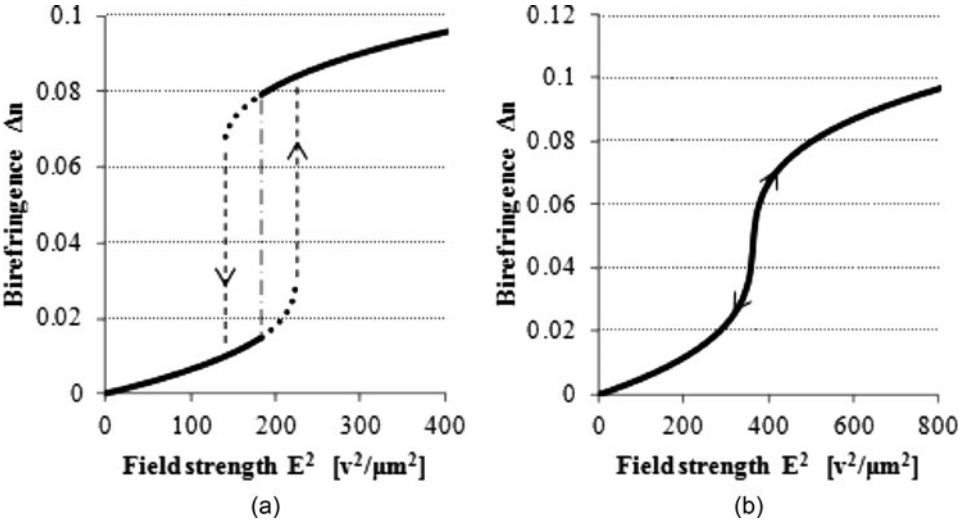

Figure 4. Numerical analysis of the electric birefringence of a nematic liquid crystal in the isotropic phase. (a) $T_{NI} < T < T_c$ (b) $T \geqq T_c$. The dotted lines in (a) correspond to the metastable state.

zero-field) and N phase. It is noted that the S coordinates of the coexisting line are S_{N-pN} given by Eq. (9). Figure 3 shows the following characteristics and qualitatively explains the experimental results very well. (i) When $E < E_c$, the S(T) curves present discontinuous pN to N transitions. (ii) At the critical field $E = E_c$, the S(T) curve passes the critical point C and the transition is of the second order. (iii) In the range of $E > E_c$, the curves always relate continuously the pN and N phases. Figure 3 with these features (i)–(iii) is analogous to the phase diagram obtained by Lelidis and Durand [12].

The observable electro-optic effect or V-Tr curves can be represented by the applied electric-field dependence of the field-induced birefringence, that can be easily calculated by converting the order parameter S(T,E) into an optical birefringence, $n = n_{||} - n_{\perp}$. Here $n_{||}$ and $n_{\perp}$ are refractive indices parallel and perpendicular to the director respectively. For a system composed of a large enough number N of anisotropic molecules, the well-known Lorentz-Lorenz formula for isotropic bodies was extended by Vuks [17] as

$$\frac{n_{||}^2 - 1}{\bar{n}^2 + 2} = \frac{1}{3} N\alpha_{||}, \quad \frac{n^2 - 1}{\bar{n}^2 + 2} = \frac{1}{3} N\alpha, \quad \bar{n}^2 = \frac{1}{3}\left(n_{||}^2 + 2n^2\right). \tag{11}$$

Thus, the refractive indices $n_{||}$ and $n_{\perp}$ for a fixed wavelength λ of the light can be numerically analyzed by using the molecular theory formulas of the electronic polarization of an ordered system composed of anisotropic molecules with a molecular polarizability (α_ℓ, α_t):

$$\alpha_{||} = \frac{1}{3}[\alpha_\ell (1 + 2S) + 2\alpha_t (1 - S)$$
$$\alpha_{\perp} = \frac{1}{3}[\alpha_\ell (1 - S) + \alpha_t (2 + S)], \tag{12}$$

together with the calculated value of S(T, E) for a thermodynamically equilibrium state. Typical results for two temperatures below and above T_c are shown in Fig. 4, where the

molecular properties (α_ℓ, α_t) are estimated to be (6.15×10^{-28}[m^3], 3.15×10^{-28}[m^3]) by referring to several experimental studies [18,19,20].

As clearly shown in Fig. 4(a), at a temperature above T_{NI} and below T_c, there exists a hysteresis due to the field-induced pN-N transition of the first order. The electric-field strength needed to make this first-order transition occur is above-mentioned E_{N-pN}, which takes a non-zero finite value in the temperature range $T_{NI} < T < T_c$ and equals to E_c at $T = T_c$. The electric birefringence effect in the low field region ($E < E_{N-pN}$), where the birefringence Δn is proportional to the square of the applied field E, corresponds to the familiar Kerr effect of nematic liquid crystals in the I phase in a strict sense. The slope λK in this part of the $\Delta n(E^2)$ curve gives the Kerr constant K at a fixed temperature in the typical order of 10^{-10} [mV^{-2}]. In the high field region ($E > E_{N-pN}$), a further large birefringence is induced because of the field stabilization of the N phase. On the other hand, at a temperature above the critical temperature ($T \geqq T_c$), the discontinuity at $E = E_{N-pN}$ vanishes and a continuous increase of the birefringence is obtained by increasing the field strength. This difference of the $\Delta n(E^2)$ curves in Figs. 4(a) and (b) provides a clear explanation of the observed results of voltage dependence of optical transmittance Tr(V) both in the low temperature and in the high temperature regions in Fig. 2.

The phase diagram in T-E plane can also be obtained as shown in Fig. 5, where the area labeled either by N or pN means that for a thermodynamically stable state and that by (N) or (pN) for a metastable state. The full line separating the regions for stable N and pN phases corresponds to the thermodynamic phase boundary. That is, the coordinates of the points on this line are $(T, E) = (T_{N-pN}, E_{N-pN})$ and the point where the line intersects the T-axis is $(T_{NI}, 0)$. Two dashed lines represent the stability limit of the super-cooled pN phase (upper line) and that of the super-heated N phase (lower line). In other words, the upper dashed line is the spinodal line separating the region for metastable pN phase from the region where pN phase is unstable. Thus, the points on this line can be $(T, E) = (T^*, E^*)$ and this spinodal line meets the T-axis at $T = T^*(0)$. Similarly, the lower dashed line is the spinodal line for metastable N phase, and the points on this line can be written as $(T, E) = (T^{**}, E^{**})$. The point where this spinodal line meets the T-axis is $T = T^{**}(0)$, giving the super-heating limit

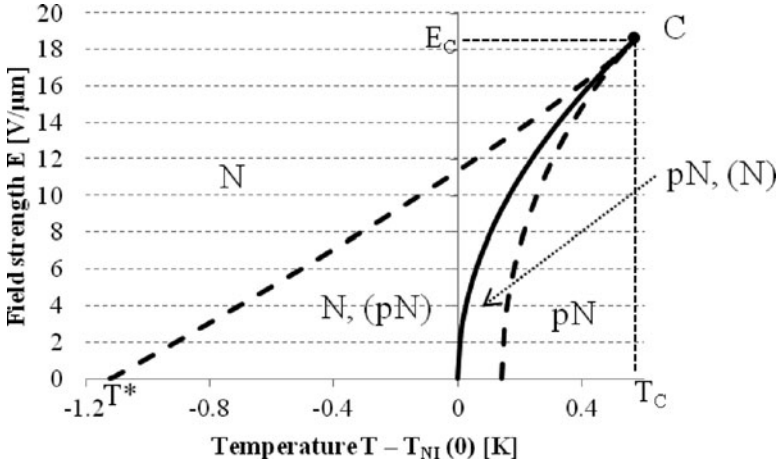

Figure 5. Phase diagram in the T-E plane. The full line corresponds to the phase boundary and the dashed lines represent the stability limits. N and pN mean stable N and pN phases and (N) and (pN) metastable N and pN phases. C is the critical point, where $S = S_c$ for $T = T_c$ and $E = E_c$.

of N phase without an electric field and making I phase absolutely stable. When $E = 0$, the stationary condition is given by

$$\partial F/\partial S = \frac{3}{4}\left[2a\left(T - T^*(0)\right) - BS + 3CS^2\right]S = 0, \tag{13}$$

which has a multiple root of $S_1 = S_2 = 0$ at $T = T^*(0)$ providing the temperature limit of a super-cooled I phase. The other real root S_3 for $T = T^*(0)$ gives the degree of order $S^*(0)$ of a stable N phase, which is easily obtained from Eq. (13) as

$$S^*(0) = \frac{B}{3C}. \tag{14}$$

On the other hand, the limiting temperature $T = T^{**}(0)$ for a super-heated N phase corresponding to the degree of order $S^{**}(0)$, gives a multiple root $S_3 = S_2$ for $\partial F/\partial S = 0$ with the other real root S_1 representing a stable I phase, that is $S_1 = 0$. From Eq.(13), it is easily found that the discriminant

$$D = B^2 - 24aC\left(T - T^*(0)\right)$$

is 0 for $T = T^{**}(0)$ and

$$\begin{aligned} T^{**}(0) &= T^*(0) + \frac{B^2}{24aC} \\ &= T_{NI} + \frac{B^2}{216aC}. \end{aligned} \tag{15}$$

The degree of order $S^{**}(0)$ for this metastable N phase at $T = T^{**}(0)$ is also obtained from Eq. (13) as

$$S^{**}(0) = \frac{B}{6C} = \frac{1}{2}S^*(0) \tag{16}$$

All the three lines meet together at a critical point C with the coordinate$(T, E) = (T_c, E_c)$, where the degree of order takes the critical value S_c (T_c, E_c). This kind of phase diagram is identical to the results of the molecular-filed description by Fan and Stephen [13] and the Landau-de Gennes approach applied to 5CB by Hornreich [11].

The characteristic lines in a phase diagram and the regions for a phase to be able to exist either in a stable state or a metastable state can also be shown in the T-S plane. The coexisting line shown by a full line in Fig. 6, which is identical to the dashed line in Fig. 3, is obtained from Eq. (9) giving two real values S_3 and S_1 for $E \geqq 0$, which satisfy $F_{S=S_1} = F_{S=S_3}$. In this case, the stationary condition $\partial F/\partial S = 0$ gives three real roots $S_1 < S_2 < S_3$, where the stationary value $F_{S=S_1} = F_{S=S_3}$ is the global minimum and $F_{S=S_2}$the local maximum. The spinodal line shown by the outer dashed line in Fig. 6 can be obtained from

$$\partial F/\partial S = -\frac{1}{3}DE^2 + \frac{3}{2}a\left(T - T^*(0)\right)S - \frac{3}{4}BS^2 + \frac{9}{4}CS^3 = 0 \tag{17a}$$

$$\partial^2 F/\partial S^2 = \frac{3}{2}a\left(T - T^*(0)\right) - \frac{3}{2}BS + \frac{27}{4}CS^2 = 0, \tag{18a}$$

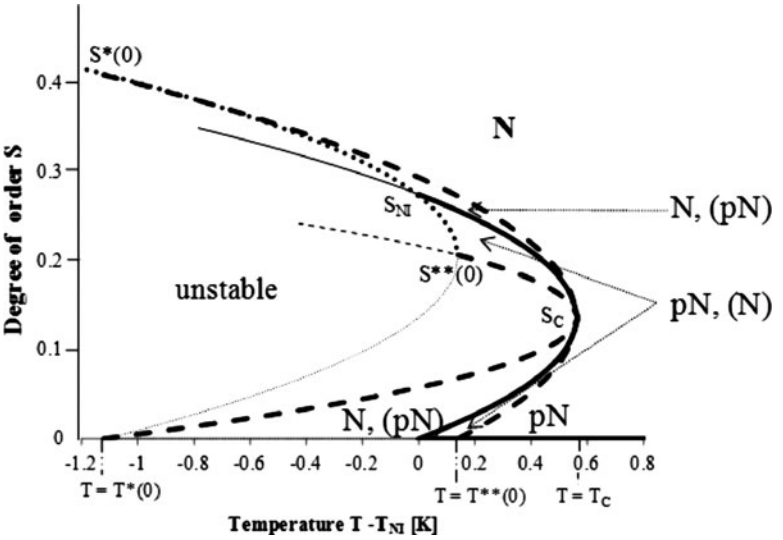

Figure 6. Phase diagram in the T-S plane. The full line corresponds to the boundary between thermodynamically stable N and pN phases. The dashed lines represent the spinodal lines with respect to metastable N and pN phases. The dotted line gives the degree of order S(T, E = 0) for N phase either in stable or metastable state.

yielding

$$E^2 = \frac{9}{4D}(B - 6CS)S^2 \tag{19}$$

and

$$2a\left(T - T^*(0)\right) - 2BS + 9CS^2 = 0. \tag{20a}$$

The roots of Eq. (20a) are given by

$$\begin{aligned} S &= \frac{B}{9C} \pm \sqrt{\frac{B^2 - 18aC\left(T - T^*(0)\right)}{81C^2}} \\ &= S_c \pm \sqrt{S_c^2 - \frac{2a}{9C}\left(T - T^*(0)\right)} \\ &= \frac{1}{2}S_{NI} \pm \sqrt{\frac{1}{3}S_{NI}^2 - \frac{2a}{9C}(T - T_{NI})}. \end{aligned} \tag{21a}$$

The two S values given by Eq. (21a) correspond to (i) the real root S_3 representing a stable N phase (the upper half of the spinodal line given by Eq. (20a)) while the multiple root $S_1 = S_2$ gives a metastable pN phase and (ii) the real root S_1 representing a stable pN phase (the lower half of the spinodal line given by Eq. (20a)) while the multiple root $S_3 = S_2$ gives a metastable N phase. The upper half of this outer spinodal line terminates at the critical point (T_c, S_c) and the point ($T^*(0)$, $S^*(0)$), while the lower half at the critical point (T_c, S_c) and the point ($T^{**}(0)$, $S^{**}(0)$). Similarly, by inserting the first equality of Eq. (15) into Eqs. (17a) and (18a), the conditions for the inner spinodal line in Fig. 6 are

obtained as

$$\partial F/\partial S = -\frac{1}{3}DE^2 + \frac{3}{2}a\left(T - T^{**}(0) + \frac{B^2}{24aC}\right)S - \frac{3}{4}BS^2 + \frac{9}{4}CS^3 = 0 \qquad (17b)$$

$$\partial^2 F/\partial S^2 = \frac{3}{2}a\left(T - T^{**}(0) + \frac{B^2}{24aC}\right) - \frac{3}{2}BS + \frac{27}{4}CS^2 = 0. \qquad (18b)$$

which yields Eq. (19) and

$$2a\left(T - T^{**}(0) + \frac{B^2}{24aC}\right) - 2BS + 9CS^2 = 0. \qquad (20b)$$

In this case, the roots of Eq. (20b) are given by

$$\begin{aligned} S &= \frac{B}{9C} \pm \sqrt{\frac{B^2 - 72aC\,(T - T^{**}(0))}{324C^2}} \\ &= S_c \pm \sqrt{\frac{1}{4}S_c^2 - \frac{2a}{9C}\left(T - T^{**}(0)\right)} \\ &= \frac{1}{2}S_{NI} \pm \sqrt{\frac{1}{12}S_{NI}^2 - \frac{2a}{9C}\,(T - T_{NI})}. \end{aligned} \qquad (21b)$$

The upper half of this inner spinodal line given by Eq. (20b) corresponds to the larger value of S (that of + sign in Eq. (21b)), which is the multiple root $S_3 = S_2$ for a metastable N phase, and the lower half corresponds to the smaller value of S (− sign in Eq. (21b)), which is the multiple root $S_1 = S_2$ for a metastable pN phase. This inner spinodal line also passes the critical point and the upper half terminates at the point ($T^{**}(0)$, $S^{**}(0)$), while the lower half at the point ($T^*(0)$, 0). The thermodynamically unstable area for any ordered state in the T-S plane ($0 \leqq S \leqq 1$) can be completely fixed with this inner spinodal line and one more line (dotted line in Fig. 6), which starts at the point ($T^*(0)$, 0) and passes the points ($T^{**}(0)$, $S^{**}(0)$), (T_{NI}, S_{NI}) and ($T^*(0)$, $S^*(0)$). Practically, the boundary is formed by the upper part of this line than the point ($T^{**}(0)$, $S^{**}(0)$). This part corresponds to the T-dependence of the degree of order S for a N phase either in a metastable or in a stable state without electric-field application, that is given by the real root S_3 of Eq. (13). It should be noted that $S^*(0)$ and $S^{**}(0)$ means the value of S(T, E) for ($T = T^*(0)$, $E = 0$) and ($T = T^{**}(0)$, $E = 0$), respectively. Figure 6 clearly shows the areas in the T-S plane for an ordered state in N and pN phases to locate under an applied electric-field either as a stable or a metastable state.

3. Wall Effects on the Electric Birefringence

By comparing the V-T_r characteristics of two kinds of cell with respect to the substrate surface treatment, it was experimentally found that the threshold voltage V_{th} observed below T_c depends on the boundary condition of the molecular alignment at the substrate surface. That is, the V_{th} value for the homeotropic cell is smaller than that of the homogeneous cell, as shown in Fig. 7. This effect is considered to be the result of the elastic consistency

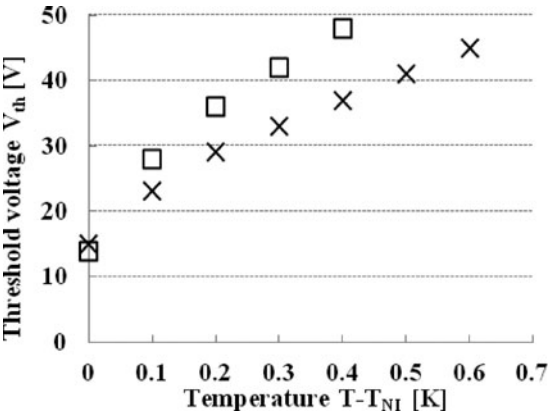

Figure 7. Temperature dependence of the threshold voltage Vth for two kinds of cell. (×; homeotropic, □; homogeneous).

between the structures of field-induced N phase in the "bulk" region and that of the zero-field pN phase formed in the interfacial region close to the substrate.

In the above analysis for the bulk state, the order parameter was assumed to be spatially uniform. However, in practical display panels with two solid substrates between which a nematic LC layer is sandwiched, there can exist an interfacial region in the nematic LC layer close to each substrate surface, where the order parameter is not necessarily spatially uniform. The thickness ζ of this interfacial region corresponds to the penetration length of the substrate surface force into the contacting nematic LC layer. That is, in one-dimensional (say z-direction) analysis, we can put a virtual interface [21] in the LC layer at a distance ζ from the substrate surface, and the order parameter on this virtual plane $S(z = \zeta)$ gives the boundary condition for the analysis of the LC layer between the two virtual interfaces, which we may call the "bulk" region. The cross-sectional view of these bulk and interfacial layers in the present model is shown in Fig. 8. The following analysis is for the interfacial region with thickness ζ, where both surface force field **h** and an electric field $\boldsymbol{E}$ act to give the thermodynamically stable state. The temperature is set to be above the field-free N-I transition temperature T_{NI}, which is marked here as T^b_{NI} to clarify that this is for the bulk region. As is well known, due to the surface field by the contacting substrate, some nematic order is induced in the interfacial region and the N-I transition temperature of the LC material in this region T^s_{NI} is usually a bit higher than T^b_{NI} [22,23]. Within a temperature range $T^b_{NI} < T < T^s_{NI}$, therefore, there exists some finite orientational order S(z) corresponding to the pN phase in the interfacial region, $0 \leqq z \leqq \zeta$, the structure of which is considered not to be spatially uniform when $S(z = 0) \neq S(z = \zeta)$. Here, at a fixed temperature, $S(z = 0) = S_s$ is assumed to be constant depending on the molecular scale interaction at the interface $z = 0$ and independent from the applied electric field. The degree of order on the virtual interface $S(z = \zeta) = S_b$ is the value of S(T, E) calculated in Sec.2. The analysis to be presented here is under the condition that an electric field is applied parallel to the z-axis and the dielectric anisotropy of the LC material is positive, and so the director $\boldsymbol{n}(z)$ in the bulk region ($z \geqq \zeta$) is assumed to be spatially uniform and parallel to the z-axis. On the contrary, the director $\boldsymbol{n}(z)$ defined for a para-nematic ordered structure in the interfacial region ($\zeta \geqq z \geqq 0$) is z-dependent except when the surface force is in the direction of the z-axis, which corresponds to the case of a homeotropically surface-treated

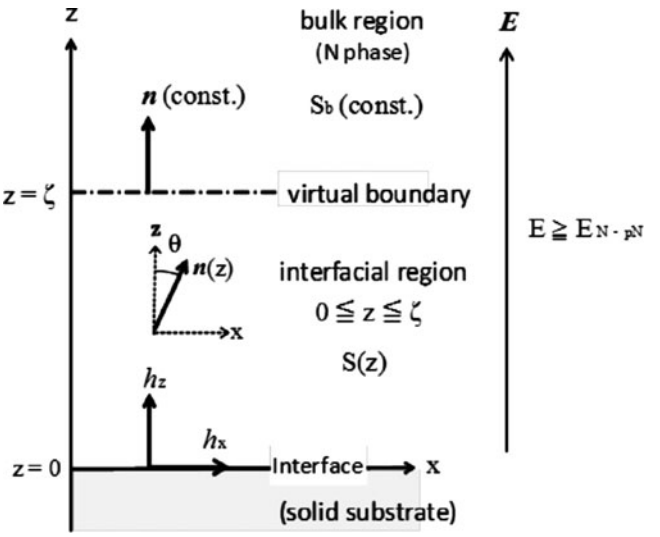

Figure 8. The bulk and interfacial regions of LC layer contacting with a flat substrate. The temperature is above the bulk transition temperature T_{NI}^{b} and below the surface transition temperature T_{NI}^{s}. Electric field $E \geqq E_{N-pN}$ is applied parallel to the z-axis so that the bulk region is in N phase with spatially uniform ($\boldsymbol{n}$, S) while both $\boldsymbol{n}$ and S in the interfacial region can be spatially non-uniform depending on the anchoring condition at the interface.

substrate. The surface field in general is tensorial and, in the case when the substrate surface has a peculiarity in the x direction, the surface field tensor has five independent elements and $h_{xy} = 0$ because of lack of the rotational symmetry around z-axis. Furthermore $h_{yz} = 0$, if the symmetry for $y \mapsto -y$ is imposed. That is, when a homogeneous rubbing treatment is applied to the substrate surface, the surface field is represented by three independent elements and is written as

$$\begin{aligned}\mathbf{h} &= h_1\left(\frac{1}{3}\mathbf{I} - \mathbf{yy}\right) + h_2(\mathbf{zz} - \mathbf{xx}) + h_3(\mathbf{xz} + \mathbf{zx}) \\ &= h_1\begin{bmatrix} 1/3 & 0 & 0 \\ 0 & -2/3 & 0 \\ 0 & 0 & 1/3 \end{bmatrix} + h_2\begin{bmatrix} -1 & 0 & 0 \\ 0 & 0 & 0 \\ 0 & 0 & 1 \end{bmatrix} + h_3\begin{bmatrix} 0 & 0 & 1 \\ 0 & 0 & 0 \\ 1 & 0 & 0 \end{bmatrix} \\ &= \begin{bmatrix} \frac{1}{3}h_1 - h_2 & 0 & h_3 \\ 0 & -\frac{2}{3}h_1 & 0 \\ h_3 & 0 & \frac{1}{3}h_1 + h_2 \end{bmatrix}.\end{aligned} \tag{22}$$

On the other hand, when a homeotropic treatment is applied, the surface field is uniaxial and $h_1 - h_2 = h_3 = 0$, that is

$$\mathbf{h} = \frac{4}{3}h_1\begin{bmatrix} -\frac{1}{2} & 0 & 0 \\ 0 & -\frac{1}{2} & 0 \\ 0 & 0 & 1 \end{bmatrix} \tag{23}$$

In the followings, two cases when **h** is given either by Eq. (22) or Eq. (23) will be analyzed by applying the phenomenological Landau-de Gennes theory to the interfacial region with

thickness ζ, which depends on T and E. In the present analysis aiming to deduce wall effects on the field strength E_{N-pN} or E_c in a semi-quantitative manner, the occurrence of the local biaxiality in the interfacial region [24,25,26] is neglected and both flexoelectric [27,28] and ordoelectric [29] effects as well.

The analysis puts the basis upon an assumption that the Landau-de Gennes theory used above to obtain $S_b(T, E)$ for a thermodynamically stable state of the bulk region can be applied to the interfacial region as well. The ground state for the interfacial region is set to that with $S(\zeta) = S_b$. The deviation of the free energy density of the interfacial region from the ground state is defined as ΔF_{int}. The deviation of total free energy density (per unit surface area) for the excited state from the ground state is now given by

$$\begin{aligned} &= {}_{\text{bulk}} + 2_{\text{interface}} \\ &= \int_{\zeta}^{d-\zeta} (F - F_0)\, dz + 2[\int_{0}^{\zeta} \Delta F_{int} dz + \int_{0}^{\zeta} \Delta F_{elec} dz]. \end{aligned} \tag{24}$$

where ΔF_{elec} is electric static energy density in the interfacial region and d is the thickness of the LC layer between two solid substrates with a flat surface. Here,

$$\text{bulk} = \int_{\zeta}^{d-\zeta} (F - F_0)\, dz$$

$$F - F_0 = \frac{3}{4} a \left(T - T^*(0)\right) S^2 - \frac{1}{4} B S^3 + \frac{9}{16} C S^4 - \frac{1}{3} D S E^2, \tag{25}$$

The tensorial order parameter $\mathbf{S}(r)$ of a LC slab is given by

$$S_{\alpha\beta}(r) = \frac{3}{2} S(r) \left(n_\alpha(r) n_\beta(r) - \frac{1}{3}\delta_{\alpha\beta}\right), \tag{26}$$

and by setting $n(z) = (n_x(z), 0, n_z(z)) = (\sin\theta(z), 0, \cos\theta(z))$,

$$\begin{aligned} S_{xx}(z) &= \frac{3}{2} S(z) \left(\sin^2\theta(z) - \frac{1}{3}\right) \\ S_{yy}(z) &= -\frac{1}{2} S(z), \\ S_{zz}(z) &= \frac{3}{2} S(z) \left(\cos^2\theta(z) - \frac{1}{3}\right), \\ S_{xz}(z) &= S_{zx}(z) = \frac{3}{4} S(z) \sin 2\theta(z), \\ S_{xy}(z) &= S_{yx}(z) = S_{yz}(z) = S_{zy}(z) = 0. \end{aligned} \tag{27}$$

Now $S_{\alpha\beta}(z)$ is assumed to be symmetric with respect to the exchange of z and $d - z$. In the temperature range of $T_{NI}^b < T < T_{NI}^s$, the interfacial free energy can be approximated [30] as

$$\int_{0}^{\zeta} \Delta F_{int} dz = \int_{0}^{\zeta} [\Delta f_0(\mathbf{S}(z)) - f_0(\mathbf{S}_b) + f_g(\dot{\mathbf{S}}(z))] dz + f_s(\mathbf{S}(0)), \tag{28}$$

where $\dot{\mathbf{S}}(z) = d\mathbf{S}(z)/dz$ and

$$f_o(\mathbf{S}(z)) = \frac{1}{2}A'S_{\alpha\beta}(z)S_{\alpha\beta}(z) + \frac{1}{3}B'S_{\alpha\beta}(z)S_{\beta\gamma}(z)S_{\gamma\alpha}(z) + \frac{1}{4}C'(S_{\alpha\beta}(z)S_{\beta\alpha}(z))^2, \quad (29)$$

$$f_g(\dot{\mathbf{S}}(z)) = \frac{1}{2}L_1'\dot{S}_{\alpha\beta}(z)\dot{S}_{\alpha\beta}(z) + \frac{1}{2}L_2'\dot{S}_{\gamma z}(z)\dot{S}_{\gamma z}(z). \quad (30)$$

Here, L_1' and L_2' are elastic constants in the pN phase. The electric-field induced pN or N phase of the present system is assumed to be uniaxial and $n(\zeta) = (\sin\theta(\zeta), 0, \cos\theta(\zeta)) = (0, 0, 1)$, that means $\theta(\zeta) = 0$ and

$$\mathbf{S}(\zeta) = \mathbf{S}_b = S(\zeta)\begin{bmatrix} -\frac{1}{2} & 0 & 0 \\ 0 & -\frac{1}{2} & 0 \\ 0 & 0 & 1 \end{bmatrix} = S_b\begin{bmatrix} -\frac{1}{2} & 0 & 0 \\ 0 & -\frac{1}{2} & 0 \\ 0 & 0 & 1 \end{bmatrix}. \quad (31)$$

For the present system, Eq. (28) means that

$$f_o(\mathbf{S}(z)) = \frac{3}{4}A'S^2 + 4B'S^3 + \frac{9}{32}C'S^4 - \frac{81}{32}(\frac{1}{3}B'S^3 - \frac{1}{2}C'S^4)\sin^2 2\theta. \quad (32)$$

Here, both S and θ are a function of z, which is not explicitly written for a simplicity sake. Now, by inserting Eq. (30) into Eq. (31), we have

$$f_o(\mathbf{S}_b) = \frac{3}{4}A'S_b^2 + 4B'S_b^3 + \frac{9}{32}C'S_b^4, \quad (33)$$

yielding

$$\begin{aligned} f_o(\mathbf{S}(z)) - f_o(\mathbf{S}_b) = {} & \frac{3}{4}A'(S^2 - S_b^2) + 4B'(S^3 - S_b^3) \\ & + \frac{9}{32}C'(S^4 - S_b^4) - \frac{81}{32}(\frac{1}{3}B'S^3 - \frac{1}{2}C'S^4)\sin^2 2\theta. \end{aligned} \quad (34)$$

Here, it is assumed that the coefficient A' is temperature dependent and B' and C' are constant.

Next, for the present system, Eq. (30) means that

$$\begin{aligned} f_g(\dot{\mathbf{S}}(z)) = {} & \frac{1}{2}L_1'[\dot{S}_{xx}(z)]^2 + \frac{1}{2}L_1'[\dot{S}_{yy}(z)]^2 + \frac{1}{2}\left(L_1' + L_2'\right)[\dot{S}_{zz}(z)]^2 \\ & + (L_1' + \frac{1}{2}L_2')[\dot{S}_{xz}(z)]^2 \\ = {} & \frac{9}{8}L_1'[\dot{S}(\sin^2\theta - \frac{1}{3}) + S\sin 2\theta\dot{\theta}]^2 + \frac{1}{8}L_1'\dot{S}^2 \\ & + \frac{9}{8}\left(L_1' + L_2'\right)[\dot{S}(\cos^2\theta - \frac{1}{3}) - S\sin 2\theta\dot{\theta}]^2 \\ & + \frac{9}{4}(L_1' + \frac{1}{2}L_2')[\frac{1}{2}\dot{S}\sin 2\theta + S\cos 2\theta\dot{\theta}]^2. \end{aligned} \quad (35)$$

Here,

$$\dot{S}_{xx}(z) = \frac{3}{2}\dot{S}(z)(\sin^2\theta(z) - \frac{1}{3}) + \frac{3}{2}S(z)\sin 2\theta(z)\,\dot{\theta}(z)\;\dot{S}_{yy}(z) = -\frac{1}{2}\dot{S}(z)$$
$$\dot{S}_{zz}(z) = \frac{3}{2}\dot{S}(z)(\cos^2\theta(z) - \frac{1}{3}) - \frac{3}{2}S(z)\sin 2\theta(z)\,\dot{\theta}(z)$$
$$\dot{S}_{xz}(z) = \dot{S}_{zx}(z) = \frac{3}{4}\dot{S}(z)\sin 2\theta(z) + \frac{3}{2}S(z)\cos 2\theta(z)\,\dot{\theta}(z) \tag{36}$$

are used for $S(z)$, $\dot{S}(z)$, $\theta(z)$, and $\dot{\theta}(z)$ by omitting (z).

By assuming that the surface free energy density f_s is given by the ordering tensor **S** at $z = 0$ as [31],

$$f_s(\mathbf{S}(0)) = c_1 S_{\alpha\beta}(0) h_\alpha h_\beta + 4c_2 S_{\alpha\beta}(0) S_{\alpha\beta}(0) + 4c_3 (S_{\alpha\beta}(0) h_\alpha h_\beta)^2$$
$$+4c_4 S_{\alpha\beta}(0) h_\beta S_{\alpha\gamma}(0) h_\gamma. \tag{37}$$

Under the assumption that **S**(z) is also uniaxial at $z = 0$, Eq. (25) is

$$S_{\alpha\beta}(0) = \frac{3}{2}S_s\left(n^s_\alpha n^s_\beta - \frac{1}{3}\delta_{\alpha\beta}\right), \tag{38}$$

where S_s and n^s is the degree of order and the director at $z = 0$, respectively. This assumption also implies $h_3 = 0$, and, from Eq. (22), $h_x = \frac{1}{3}h_1 - h_2$, $h_y = -\frac{2}{3}h_1$, $h_z = \frac{1}{3}h_1 + h_2$for the homogeneous alignment case and, from Eq. (23), $h_x = h_y = -\frac{2}{3}h_1$, $h_z = \frac{4}{3}h_1$ for the homeotropic case.

(i) homeotropic case

The director n^s is assumed to be parallel to the z-axis and $n^s_x = n^s_y = 0$, $n^s_z = 1$, resulting in $S_{xx}(0) = S_{yy}(0) = -\frac{1}{2}S_s$, $S_{zz}(0) = S_s$. The surface free energy density is now

$$f_s(\mathbf{S}(0)) = \frac{4}{3}c_1 h_1^2 S_s + (6c_2 + \frac{64}{9}c_3 h_1^4 + 8c_4 h_1^2)S_s^2. \tag{39}$$

(ii) homogeneous case

The director n^s is assumed to be parallel to the x-axis and $n^s_x = 1, n^s_y = n^s_z = 0$, resulting in $S_{xx}(0) = S_s$, $S_{yy}(0) = S_{zz}(0) = -\frac{1}{2}S_s$. Then, the surface free energy density is

$$f_s(\mathbf{S}(0)) = c_1 h_a S_s + (6c_2 + 4c_3 h_a^2 + 4c_4 h_b)S_s^2, \tag{40}$$

where

$$h_a h_x^2 - \frac{1}{2}(h_y^2 + h_z^2) = -\frac{3}{18}h_1^2 + \frac{1}{2}h_2^2 - h_1 h_2,$$
$$h_b h_x^2 + \frac{1}{4}(h_y^2 + h_z^2) = \frac{1}{4}h_1^2 + \frac{5}{4}h_2^2 - \frac{1}{2}h_1 h_2,$$

which is simplified as

$$f_s(\mathbf{S}(0)) = H_a S_s + H_b S_s^2 \tag{41}$$

by defining the surface anchoring coefficients, $H_a c_1 h_a$ and $H_b 6c_2 + 4c_3 h_a^2 + 4c_4 h_b$.

Finally, the electric static energy density ΔF_{elec} under an applied field $\boldsymbol{E}$ parallel to the z-axis is given by

$$\begin{aligned}\Delta F_{elec} &= -\frac{1}{3}D'(S_{zz}(z) - S_b)E^2 \\ &= -D'[\frac{1}{2}S(\cos^2\theta - \frac{1}{3}) - \frac{1}{3}S_b]E^2. \end{aligned} \tag{42}$$

To sum up, each term of the right-hand side of $_{-interface}$:

$$_{-interface} = \int_0^{\zeta} \left[f_o(\mathbf{S}(z)) - f_o(\mathbf{S}_b) + f_g\left(\dot{\mathbf{S}}(z)\right) + F_{elec}\right] dz + f_s(\mathbf{S}(0)). \tag{43}$$

is given as follows, depending on the substrate surface treatment.
(i) homeotropic case ($\theta(\mathbf{z}) = 0$)

$$\begin{aligned} f_o(\mathbf{S}(z)) - f_o(\mathbf{S}_b) &= \frac{3}{4}A'(S^2 - S_b^2) + 4B'(S^3 - S_b^3) + \frac{9}{32}C'(S^4 - S_b^4) \\ f_g(\dot{\mathbf{S}}(z)) &= \frac{3}{4}(L_1' + \frac{2}{3}L_2')\dot{S}^2 \\ F_{elec} &= -\frac{1}{3}D'(S - S_b)E^2 \\ f_s(\mathbf{S}(0)) &= H_1 S_s + H_2 S_s^2. \end{aligned} \tag{44}$$

In the numerical analysis, the degree of order at the substrate surface S_s is given as a fixed boundary condition, which can be reasonably large. By taking this condition into account, the spatial distribution of S(z) in the interfacial region ($0 \leqq z \leqq \zeta$) can be calculated to minimize the interfacial free energy per unit area $_{interface}$ by solving the Euler-Lagrange equation in terms of the functional S(z) with the boundary conditions at $z = \zeta$ and $z = 0$ ($S(0) = S_s$). The parameters to be given in the practical numerical analysis are $A'\left(= a'(T - T_s^*(0))\right)$, B', C', D', L_1', L_2' and the surface anchoring coefficients (H_1, H_2). The prime means their values in the interfacial region, which are considered to be different from those in the bulk region because of the contribution of interactions between the LC molecules and the molecules covering the substrate surface. Similar to the surface transition temperature T_{NI}^s, the super-cooling limit of the I phase in the interfacial region may be different from its bulk value and so is marked here as $T_s^*(0)$.
(ii) homogeneous case

$$\begin{aligned} f_o(\mathbf{S}(z)) - f_o(\mathbf{S}_b) &= \frac{3}{4}A'(S^2 - S_b^2) + 4B'(S^3 - S_b^3) + \frac{9}{32}C'(S^4 - S_b^4) \\ &\quad -\frac{81}{32}(\frac{1}{3}B'S^3 - \frac{1}{2}C'S^4)\sin^2 2\theta \\ f_g(\dot{\mathbf{S}}(z)) &= \frac{9}{8}L_1'[\dot{S}(\sin^2\theta - \frac{1}{3}) + S\sin 2\theta\dot{\theta}]^2 + \frac{1}{8}L_1'\dot{S}^2 \\ &\quad +\frac{9}{8}\left(L_1' + L_2'\right)[\dot{S}(\cos^2\theta - \frac{1}{3}) - S\sin 2\theta\dot{\theta}]^2 \end{aligned}$$

$$+\frac{9}{4}(L_1^{'}+\frac{1}{2}L_2^{'})[\frac{1}{2}\dot{S}\sin 2\theta + S\cos 2\theta\dot{\theta}]^2$$

$$\Delta F_{elec} = -D^{'}[\frac{1}{2}S(\cos^2\theta - \frac{1}{3}) - \frac{1}{3}S_b]E^2$$

$$f_s(\mathbf{S}(0)) = H_a S_s + H_b S_s^2. \tag{45}$$

In addition to the spatial distribution of the degree of order S(z), that of the director orientation θ(z) can be obtained by taking into account the Euler-Lagrange equation in terms of the functional θ(z) with the boundary conditions at z = 0 and z = ζ, too. Besides the difference in the surface free energy density $f_s(\mathbf{S}(0))$, the key factor of the observable change of the threshold voltage depending on the substrate surface treatment is considered to be the contribution of $f_g(\dot{\mathbf{S}}(z))$ term, which consists of quadratic functions of$\dot{\theta}$(z) as seen in Eq. (45). The difference of $f_g(\dot{\mathbf{S}}(z))$ between the homogeneous and homeotropic cases is calculated as

$$\Delta\text{homog} - \text{homeof}_g(\dot{\mathbf{S}}(z)) = \frac{3}{8}[3\left(2L_1^{'} + L_2^{'}\right)S^2\dot{\theta}^2 - L_2^{'}(\dot{S}^2\sin^2\theta + S\dot{S}\dot{\theta}\sin 2\theta, \tag{46}$$

which is simplified in the one-constant approximation, $L_1' = L_2' = L'$, as

$$\Delta\text{homog} - \text{homeof}_g(\dot{\mathbf{S}}(z)) = \frac{3}{8}[9S^2\dot{\theta}^2 - (\dot{S}^2\sin^2\theta + S\dot{S}\dot{\theta}\sin 2\theta)]L^{'}. \tag{47}$$

It should be noted here that the spatial distribution of **S**(z) in the interfacial region minimizing $_{-\text{interface}}$ with the boundary condition $S(\zeta) = S_b$ does not correspond to the thermodynamically equilibrium state of the LC layer under an applied field with the boundary conditions $S(0) = S(d) = S_s$. However, the difference of the minimum $_{-\text{interface}}$ mainly due to the gradient term $f_g(\dot{\mathbf{S}}(z))$ can qualitatively explain the higher threshold voltage of the homogeneous LC cell compared to the homeotropic cell as an excess energy to compensate the free energy increase caused by the deformation of director field $\dot{\theta}$(z) in the interfacial region.

4. Summary

The electric birefringence effect of nematic liquid crystals in the isotropic phase, which looks promising to be applied to novel liquid crystal displays with features of fast switching [32], was analytically described with respect to the statics. Here, the Landau-de Gennes theory of nematic-isotropic phase transition was used to obtain the thermodynamically equilibrium state of an electric-field induced para-nematic or nematic phase. The optical birefringence of the ordered state was analyzed by using the extended Lorentz-Lorenz formula by Vuks and the molecular theory formulas of electronic polarization. In addition, the boundary effects on the threshold phenomenon of electric birefringence were qualitatively analyzed by assuming that, near the solid-substrate surface, an interfacial region exists with thickness ζ corresponding to the penetration length of the substrate surface force into the contacting LC layer. Even when the bulk region of the LC layer is in isotropic phase, the surface force can induce a short-range orientational-order in the interfacial region. The order parameter is not necessarily spatially uniform in this region and the director on the geometrical interface at the substrate surface depends on the surface treatment, that makes the free energy density of the interfacial region differ depending on the treatment. The Landau-de

Gennes model was also applied to the interfacial region to yield the Euler-Lagrange equation giving the distribution of tensorial order parameter. The elastic deformation energy in the interfacial region, together with the surface energy of the geometrical interface, is qualitatively shown to play the key role in the experimentally observed dependence of the threshold voltage on the substrate surface treatment.

The present analysis is considered to be of great help to improve the display performance of the novel liquid-crystal device using electric birefringence effect and to optimize the display panel design as well.

References

[1] Kikuchi, H., Yokota, H., Hisakado, Y., Yang, H., & Kajiyama, T. (2002). Polymer-stabilized liquid crystal blue phases. *Nat. Mater.*, *1*, 64–68.

[2] He, S., Lee, J.-H., Cheng, H.-C., Yan, J., & Wu, S.-T. (2012). Fast-Response Blue-Phase Liquid Crystal for Color-Sequential Projection Displays. *J. Disp. Tech.*, *8*, 352–356.

[3] Patel, J. S., & Meyer, R. B. (1987). Flexoelectric Electro-optics of a Cholesteric Liquid Crystal. *Phys. Rev. Lett.*, *58*, 1538–1540.

[4] Lee, H. H., Yu, J.-S., Kim, J.-H., Yamamoto, S., & Kikuchi, H. (2009). Fast electro-optic device controlled by dielectric response of planarly aligned cholesteric liquid crystals. *J. Appl. Phys.*, *106*, 014503.

[5] Gardiner, D. J., Morris, S. M., Hands, P. J., Castles, F., Qasim, M. M., Kim, W.-S., Choi, S. S., Wilkinson, T. D., & Coles, H. J. (2012). Spontaneous induction of the uniform lying helix alignment in bimesogenicliquid crystals for the flexoelectro-optic effect. *Appl. Phys. Lett.*, *100*, 063501.

[6] Panov, V. P., Balachandran, R., Nagaraj, M., Vij, J. K., Tamba, M. G., Kohlmeierand, A., & Mehl, G. H. (2011). Fast electro-optic device controlled by dielectric response of planarly aligned cholesteric liquid crystals. *Appl. Phys. Lett.*, *99*, 261903.

[7] Gardiner, D. J., Morris, S. M., Hands, P. J., Castles, F., Qasim, M. M., Kim, W.-S., Choi, S. S., Wilkinson, T. D., & Coles, H. J. (2011). Polymer stabilized chiral nematic liquid crystals for fast switching and high contrast electro-optic devices. *Appl. Phys. Lett.*, *98*, 263508.

[8] Kosuge, M., Naemura, S., Koma, N., Tsuyuki, T., & Fujimura, K. (2009). Feasibility study on fast-switching liquid-crystal display using field-induced nematic orientational order. *Proceedings of 11th Asian Symp. Info. Display*, 89–92.

[9] Kosuge, M., Naemura, S., Koma, N., Tsuyuki, T., & Fujimura, K. (2010). Experiment-based proposal of novel fast-switching liquid-crystal displays using field-induced isotropic-nematic transition. *Proceedings of 17th IDW*, 1783–1786.

[10] Nicastro, A. J., & Keyes, P. H. (1984). Electric-field-induced critical phenomena at the nematic-isotropic transition and the nematic-isotropic critical point. *Phys. Rev. A*, *30*, 3156–3160.

[11] Hornreich, R. M. (1985). Landau theory of the isotropic-nematic critical point. *Phys. Lett.*, *109A*, 232–234.

[12] Lelidis, I., & Durand, G. (1993). Electric-field-induced isotropic-nematic phase transition. *Phys. Rev. E*, *48*, 3822–3824.

[13] Fan, C., & Stephen, M. J. (1970). Isotropic-nematic phase transition in liquid crystals. *Phys. Rev. Lett.*, *25*, 500–503.

[14] Hanus, J. (1969). Effect of the molecular interaction between anisotropic molecules on the optical kerr effect. Field-induced phase transition. *Phys. Rev.*, *178*, 420–428.

[15] de Gennes, P. G. (1969). Phenomenology of short-range-order effects in the isotropic phase of nematic materials. *Phys. Lett.*, *30A*, 454–455.

[16] Coles, H. J. (1978). Laser and electric field induced birefringence studies on the cyanobiphenyl homologues. *Mol. Cryst. Liq. Cryst. Lett.*, *49*, 67–74.

[17] Vuks, M. V. (1966). Determination of optical anisotropy of aromatic molecules from double refraction in crystal. *Opt. Specktrosk.*, *20*, 644 [Engl. Trans. in *Opt. Spectrosc.*, *20*, 361–368 (1966)].
[18] Dunmur, D. A., Manterfield, M. R., Miller, W. H., & Dunleavy, J. K. (1978). The dielectric and optical properties of the homologous series of cyano-alkyl-biphenyl liquid crystals. *Mol. Cryst. Liq. Cryst.*, *45*, 127–144.
[19] Yokota, K., Shioda, T., Nakata, M., Takanishi, Y., Ishikawa, K., Takezoe, H., Ishitobi, M., & Sekine, C. (2003). Experimental determination of molecular polarizability anisotropy of nematogens by depolarized rayleigh light scattering. *Liq. Cryst.*, *30*, 697–700.
[20] Li, J., & Wu, S.-T. (2004). Self-consistency of Vuks equations for liquid-crystal refractive indices. *J. Appl. Phys.*, *96*, 6253–6258.
[21] Jérôme, B. (1991). Surface effects and anchoring in liquid crystals. *Rep. Prog. Phys.*, *54*, 391–452.
[22] Sheng, P. (1976). Phase transition in surface-aligned nematic films. *Phys. Rev. Lett.*, *37*, 1059–1062.
[23] Sheng, P. (1982). Boundary-layer phase transition in nematic liquid crystals. *Phys. Rev. A*, *26*, 1610–1617.
[24] Lubensky, T. C. (1970). Molecular description of nematic liquid crystals. *Phys. Rev. A*, *2*, 2497–2514.
[25] Sluckin, T. J., & Poniewierski, A. (1985). Novel surface phase transition in nematic liquid crystals: Wetting and the Kosterlitz-Thouless transition. *Phys. Rev. Lett.*, *55*, 2907–2910.
[26] Sen, A. K., & Sullivan, D. E. (1987). Landau-de Gennes theory of wetting and orientational transitions at a nematic-liquid-substrate interface. *Phys. Rev. A*, *35*, 1391–1403.
[27] Derzhanskii, A. I., & Petrov, A. G. (1979). Flexoelectricity in nematic liquid crystals. *Acta Phys. Pol. A*, *55*, 747–767.
[28] Osipov, M. A. (1984). The order parameter dependence of the flexoelectric coefficients in nematic liquid crystals. *J. Phys. Lett. (Paris)*, *45*, L823–L826.
[29] Barbero, G., Dozov, I., Palierne, J. F., & Durand, G. (1986). Order electricity and surface orientation in nematic liquid crystals. *Phys. Rev. Lett.*, *56*, 2056–2059.
[30] Sluckin, T. J., & Poniewierski, A. (1986). Orientational wetting transitions and related phenomena in nematics. In: *Fluid Interfacial Phenomena*, Croxton, C. A. (Ed.), Chapter 5, Wiley: New York, 215.
[31] Pandit, R., & Wortis, M. (1982). Surfaces and interfaces of lattice models: Mean-field theory as an area-preserving map. *Phys. Rev. B*, *25*, 3226–3241.
[32] Kosuge, M., Naemura, S., & Fujimura, K. (submitted, 2012). Feasibility study of novel fast-switching liquid-crystal displays using electric birefringence effect. *J. Soc. Info. Display.*